A hidden incoherent switch regulates RCAN1 in the calcineurin–NFAT signaling network

Sung-Young Shin[1,*], Hee Won Yang[2,*], Jeong-Rae Kim[1,3], Won Do Heo[2,‡] and Kwang-Hyun Cho[1,‡]

[1]Department of Bio and Brain Engineering, [2]Department of Biological Sciences, Korea Advanced Institute of Science and Technology (KAIST), Daejeon 305-701, Republic of Korea
[3]Department of Mathematics, University of Seoul, Seoul 130-743, Republic of Korea

*These authors contributed equally to this work
‡Authors for correspondence (wdheo@kaist.ac.kr; ckh@kaist.ac.kr)

Accepted 15 September 2010
Journal of Cell Science 124, 82-90

doi:10.1242/jcs.076034

Summary

Regulator of calcineurin 1 (RCAN1) is a key regulator of the calcineurin–NFAT signaling network in organisms ranging from yeast to human, but its functional role is still under debate because different roles of RCAN1 have been suggested under various experimental conditions. To elucidate the mechanisms underlying the RCAN1 regulatory system, we used a systems approach by combining single-cell experimentation with in silico simulations. In particular, we found that the nuclear export of GSK3β, which switches on the facilitative role of RCAN1 in the calcineurin–NFAT signaling pathway, is promoted by PI3K signaling. Based on this, along with integrated information from previous experiments, we developed a mathematical model in which the functional role of RCAN1 changes in a dose-dependent manner: RCAN1 functions as an inhibitor when its levels are low, but as a facilitator when its levels are high. Furthermore, we identified a hidden incoherent regulation switch that mediates this role change, which entails negative regulation through RCAN1 binding to calcineurin and positive regulation through sequential phosphorylation of RCAN1.

Key words: Systems biology, Calcineurin–NFAT signaling pathway, RCAN1, Incoherent regulation switch, Cardiac hypertrophy, Mathematical modeling

Introduction

The calcineurin–nuclear factor of activated T-cells (NFAT) signaling pathway has essential roles in many physiological processes, including T-cell activation, memory formation and apoptosis in neurons, and growth and differentiation in skeletal muscle and cardiac cells (Rusnak and Mertz, 2000; Shin et al., 2006; Shin et al., 2008; Tomida et al., 2003). In the calcineurin–NFAT signaling pathway, calcineurin is activated by Ca^{2+} binding to calmodulin. The activated calcineurin dephosphorylates NFAT, leading to its nuclear localization and subsequent activation of its target genes (Liang et al., 2003; Rusnak and Mertz, 2000; Vega et al., 2003a). Regulator of calcineurin 1 (RCAN1), a protein encoded by one of the target genes of NFAT, binds and inhibits calcineurin (Chan et al., 2005; Vega et al., 2002). However, recent studies have shown that RCAN1 facilitates calcineurin–NFAT signaling under various experimental conditions, and this has led to controversy regarding the functional role of RCAN1 (Fox and Heitman, 2005; Sanna et al., 2006; Vega et al., 2003b) (Table 1). For instance, Vega and colleagues suggested a dual role of RCAN1 in the development of cardiac hypertrophy (Vega et al., 2003b), whereas Sanna and co-workers insisted that RCAN1 functions only as a calcineurin facilitator and reasoned that previous experiments showing RCAN1 to be a calcineurin inhibitor might be due to sequestration effects resulting from an overexpression approach (Sanna et al., 2006). We note, however, that Hoeffer (Hoeffer et al., 2007) and Ryeom and colleagues (Ryeom et al., 2003) demonstrated an inhibitory role of RCAN1 in mouse knockout experiments.

In spite of such diverse and conflicting lines of evidence regarding the regulatory mechanism of calcineurin–NFAT signaling, there has been no attempt to explain the role change of RCAN1 from a system-level perspective by integrating all available experimental evidence. Therefore, we used a systems approach in the present study by combining single-cell experimentation and in silico simulations to elucidate why different roles of RCAN1 have been suggested depending on the experimental conditions. For in silico simulations, we developed a mathematical model based on our own experimentation, as well as integrated information from previous experiments, encompassing calcineurin–NFAT signaling, RCAN1 regulatory processes, crosstalk mediated through extracellular signal-regulated kinase (ERK) and phosphatidylinositol 3-kinase (PI3K) signaling pathways, and the glycogen synthase kinase 3β (GSK3β) translocation mechanism.

As a result, we found that PI3K signaling promotes the nuclear export of GSK3β. Moreover, from extensive in silico simulations, we found that the functional role of RCAN1 changes in a dose-dependent manner: RCAN1 functions as an inhibitor when its levels are low, but as a facilitator when its levels are high. Furthermore, we have identified a hidden incoherent regulation switch that coordinates such a role change via an intricate balance between positive (sequential phosphorylation of RCAN1) and negative (RCAN1 binding to calcineurin) regulation.

Results

A mathematical model of the calcineurin–NFAT signaling network

We developed a mathematical model to describe the calcineurin–NFAT signaling network based on information from previous experiments, including our own. This model encompasses the calcineurin–NFAT signaling pathway, RCAN regulation module

Journal of Cell Science

Table 1. Different reported roles of RCAN1

Suggested role	Experimental condition	Experimental observations	References
Facilitative	RCAN1/2 knockout	Mouse embryonic fibroblasts deficient in RCAN1 and RCAN2 show impaired activation of NFAT	(Sanna et al., 2006).
	RCAN1/2 knockout	Hearts of mice deficient in RCAN1 and RCAN2 do not show hypertrophy in response to 2 weeks of infusion of PE plus AngII	(Sanna et al., 2006)
	RCAN1 knockout	RCAN1 mutant strains unable to filament in a bilateral mutant cross in *Cryptococcus neoformans*, indicating that RCAN1, in addition to calcineurin, is required for mating	(Fox and Heitman, 2005)
	RCAN1 knockout	Cardiac hypertrophy in response to pressure overload or chronic adrenergic stimulation blunted in RCAN1-knockout mice	(Vega et al., 2003b)
Inhibitory	RCAN1 knockout	RCAN1-knockout mice display increased enzymatic calcineurin activity in the hippocampus	(Hoeffer et al., 2007)
	RCAN1 knockout	RCAN1-deficient T cells show transactivation thresholds that were shifted substantially to lower strengths of T cell receptor (TCR) signaling	(Ryeom et al., 2003)
	RCAN1 overexpression (2.4-fold increase in *Rcan1* mRNA)	After VEGF treatment, endothelial cells isolated from RCAN1 transgenic mice exhibit predominantly cytoplasmic NF-ATc1 localization	(Baek et al., 2009)
	RCAN1 overexpression (transgenic mouse model)	Transgenic mice expressing cDNA encoding human *RCAN1* in the myocardium show blunted hypertrophic response	(Hill et al., 2002)
	RCAN1 overexpression (in vitro model)	Constitutive expression of RCAN1 in endothelial cells markedly impaired NF-ATc nuclear localization, proliferation and tube formation	(Minami et al., 2004)

and the PI3K signaling pathway (Fig. 1). Below, we describe the major signaling processes that are considered in our model.

The calcineurin–NFAT signaling pathway is activated by an increase in the cytosolic Ca^{2+} level. Ca^{2+} binds to the catalytic subunit of calcineurin through calmodulin, which leads to dephosphorylation of cytosolic NFAT and promotion of its nuclear translocation (Rusnak and Mertz, 2000; Vega et al., 2003a). Although NFAT has several serine phosphorylation sites (Chow and Davis, 2000), in this model these were represented by a single, virtual phosphorylation site. Nuclear NFAT, in cooperation with GATA4 (Tokudome et al., 2005), activates transcription of various hypertrophy-related genes, including those encoding atrial natriuretic peptide (ANP), brain natriuretic peptide (BNP) and RCAN1; however, only RCAN1 was considered in this model because the other proteins do not regulate calcineurin–NFAT signaling. It should be noted that RCAN1 has several splice variants and, among these, RCAN1.1 and RCAN1.4 are most abundant in cardiac cells (Dey et al., 2007). Only RCAN1.4 is induced by NFAT (Dey et al., 2007). Thus, hereafter RCAN1 refers to RCAN1.4, unless otherwise mentioned. RCAN1 competitively binds to and inhibits calcineurin activity through the region encoded by exon 7, which results in negative feedback regulation (Chan et al., 2005). In this model, RCAN1 is considered to be a multi-phosphoprotein that is sequentially phosphorylated by ERKs and GSK3β (Hilioti et al., 2004; Vega et al., 2002). The functional impact of RCAN1 on induction of nuclear NFAT varies depending on the phosphorylation state of RCAN1 (Abbasi et al., 2006). For instance, Abbasi and colleagues showed that RCAN1 dissociates from calcineurin if RCAN1 is phosphorylated at Ser112 by ERK5, and that calcineurin–NFAT signaling is then re-established (Abbasi et al., 2006). However, the effect of RCAN1 phosphorylation by ERK1 and ERK2 (ERK1/2) on calcineurin–NFAT signaling has not yet been described. From our experiments, we confirmed that the MEK1 and MEK2 (MEK1/2) inhibitor U0126 also suppresses the nuclear localization of NFAT in H9C2 cells, after treatment of the cells with the Ca^{2+} activator ionomycin (supplementary material Fig. S1A,B). Taken together, these results imply that the effects of ERK1/2 and ERK5 are functionally the same. Thus, in this model we denote ERK1/2 and ERK5 by ERK, without any discrimination. RCAN1 phosphorylated at Ser112 by ERK is further phosphorylated at Ser108 by GSK3β, but calcineurin selectively removes the phosphate at Ser108 of RCAN1 (Vega et al., 2002).

GSK3β can be localized to the cytosol or nucleus (Haq et al., 2000; Morisco et al., 2001), but its functional effect on calcineurin–NFAT signaling changes depending on its localization. In the cytosol, GSK3β can re-establish calcineurin–NFAT signaling through the sequential phosphorylation of RCAN1 in cooperation with ERK, but in the nucleus, calcineurin–NFAT signaling is inhibited through NFAT phosphorylation by GSK3β. In addition, NFAT phosphorylated by GSK3β in the cytosol binds to 14-3-3 protein, which enhances inhibition of the nuclear localization of NFAT (Chow and Davis, 2000; Du et al., 2005; Liao et al., 2005). In this model, we have simplified the sequential multi-step processes of NFAT translocation mediated by GSK3β to a single, semi-mechanistic step. Although localization of GSK3β has an important role in calcineurin–NFAT signaling, the underlying regulatory mechanism is not fully understood. In this study, we show that the nuclear export of GSK3β is promoted by the PI3K signaling pathway (see the following section for details), and this finding was incorporated into the model.

The mathematical model comprises 24 ordinary differential equations and 57 kinetic parameters (supplementary material Tables S1–S7). The kinetic parameter values were estimated using both our own experimental data and those previously obtained by others, as a training data set. The kinetic parameter values of the calcineurin–NFAT pathway were estimated based on the time course data of nuclear NFAT induction after platelet-derived growth factor (PDGF) treatment of H9C2 cells (supplementary material Fig. S1C). The transcriptional time delay – the time taken for *Rcan1* induction up to the level of statistical significance ($P<0.05$) after ionomycin (IM) treatment – was estimated to be about 30 minutes based on real-time PCR data (supplementary material Fig. S1D,E). The kinetic parameters of the ERK and PI3K signaling pathways were fitted to previous experimental data (Aoki et al., 2000; Clerk et al., 2006; Markou et al., 2008; Morisco et al., 2008; Morisco et al., 2000; Morris et al., 2005; Tian et al., 2003; Yin et al., 2006), as well

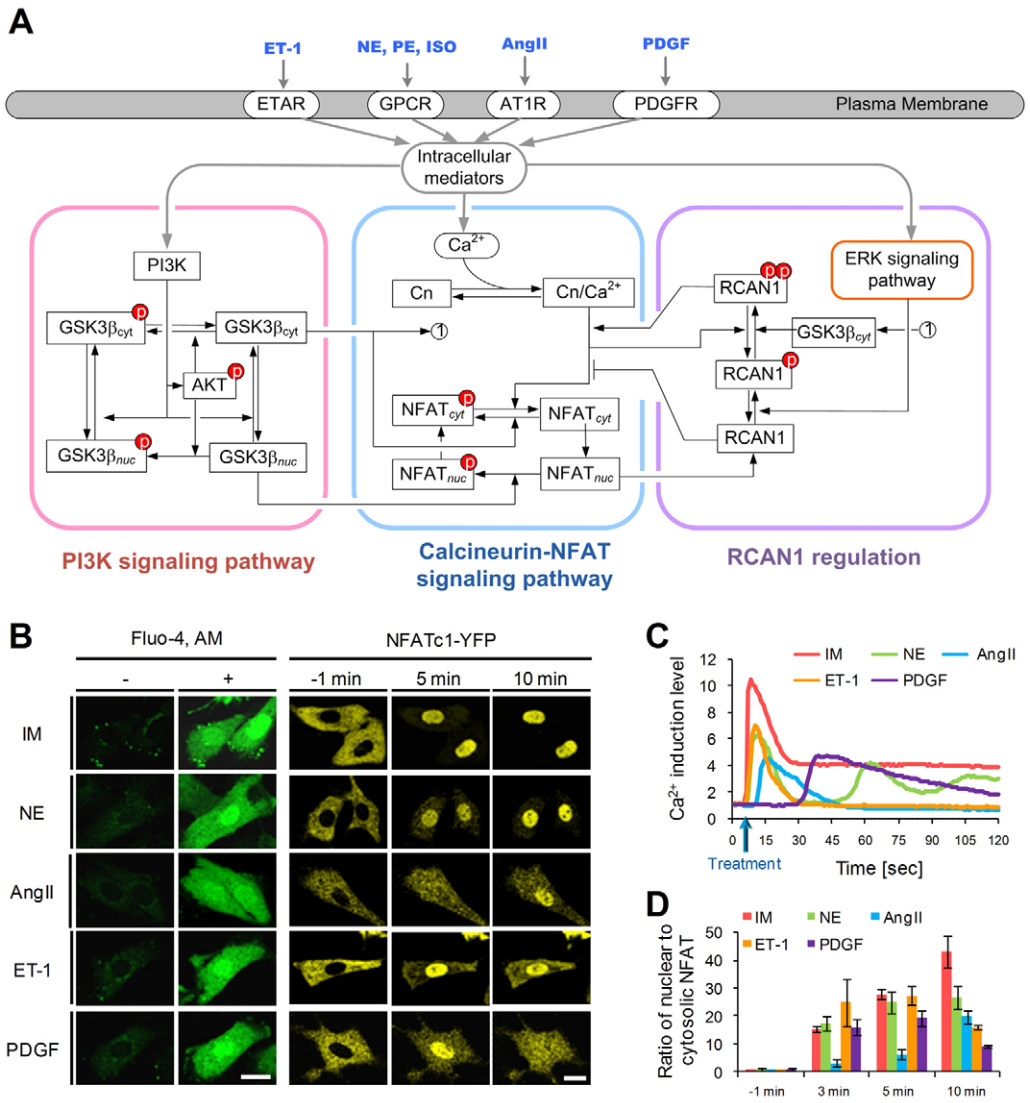

Fig. 1. The calcineurin–NFAT signaling network. (**A**) A schematic diagram of the network. (**B**) Ca^{2+} levels and nuclear NFAT translocation were measured for IM (1 μM), ET-1 (200 nM), NE (100 μM), AngII (200 nM) and PDGF (5 nM). Ca^{2+} levels were measured using Fluo-4 Ca^{2+} chelating. Scale bars: 20 μm. (**C**) Quantification of the Ca^{2+} induction shown in B. Relative fluorescence units (RFU) are normalized to the fluorescence before induction. (**D**) Quantitative measurement of the NFATc1–YFP translocation shown in B. The ratio of nuclear to cytosolic NFAT is normalized by the initial value: $(F_{1Nuc}/F_{1Cyt})/(F_{0Nuc}/F_{0Cyt})$ where F_0 and F_1 are the fluorescent intensities before and after, respectively, treatment with hypertrophic stimulants (n=2, error bars indicate s.d.).

as to our own data (supplementary material Fig. S2 and Fig. S3A,B). We note that the time profiles of phosphorylated ERK, Akt and GSK3β are quite different depending on the hypertrophic stimulants used, such as PDGF, angiotensin II (AngII), phenylephrine (PE), isoproterenol (ISO) and endothelin-1 (ET-1) (supplementary material Fig. S2), because these stimulants all have different input points (i.e. receptors) and intercellular mediators through which the signals pass to the ERK and PI3K signaling pathways. In the model, we did not take into account all the detailed variations from the input to the major signaling pathways involving the various mediators that differed according to the hypertrophic stimulant used. Instead, we constructed a common minimal model of the major ERK and PI3K signaling pathways and estimated the condition-specific kinetic parameter values based on the experimental data obtained for each hypertrophic stimulant. The kinetic parameters of the RCAN1 regulation module were fitted to the experimental data obtained from rat neonatal cardiac myocytes (Abbasi et al., 2005) (supplementary material Fig. S3C,D). We confirmed that all the simulation results were quantitatively consistent with the training data set (supplementary material Fig. S1C–E, Fig. S2 and Fig. S3C–E).

To validate the responses of the calcineurin–NFAT signaling network to typical hypertrophic stimulants such as norepinephrine (NE), AngII, ET-1 and PDGF, we determined the induction levels of cytosolic Ca^{2+} and NFAT translocation to the nucleus using H9C2 cells, where IM was used as the positive control. All the examined hypertrophic stimulants increased the Ca^{2+} levels, which were measured using the Ca^{2+}-chelating dye Fluo-4 (Fig. 1B,C). To investigate the dynamics of NFAT translocation to the nucleus, the cells were transfected with NFATc1–YFP. After treatment with the various hypertrophic stimulants, NFATc1–YFP was found to be imported to the nucleus (Fig. 1B,D and supplementary material

Movie 1). The translocation of NFATc1–YFP corresponded to the increasing cytosolic Ca^{2+} levels. Taken together, these results confirm that in H9C2 cells, these typical hypertrophic stimulants induce an increase in cytosolic Ca^{2+} levels and thereby nuclear NFAT localization.

PI3K induces the nuclear export of GSK3β

The translocation mechanism of GSK3β in cardiac cells is not yet fully understood. Several conflicting experimental results have been reported: for example, ISO induces nuclear export of GSK3β (Morisco et al., 2001), whereas ET-1 induces pronounced translocation of GSK3β to the nucleus (Haq et al., 2000). Because GSK3β is regulated by PI3K signaling and is exported from the nucleus to the cytosol by nuclear export signal (NES)-containing proteins such as FRAT1 and Axin2 (Franca-Koh et al., 2002; Yook et al., 2006), we hypothesize that the localization of GSK3β is regulated by PI3K signaling and NES-containing proteins. To investigate this possibility, cells were stained with GSK3β antibody and transfected with YFP–GSK3β and YFP–GSK3β^{S9A} (a form insensitive to PI3K). Without serum deprivation, both endogenous and overexpressed GSK3β were localized to the cytosol, whereas endogenous GSK3β was accumulated in the nucleus following pre-incubation for 1 hour with the PI3K-specific inhibitor LY294002 (LY29) or the Crm1-specific inhibitor leptomycin B (LMB) (Fig. 2A,B).

To investigate whether translocation of GSK3β is directly regulated by PI3K through phosphorylation of GSK3β at Ser9, cells co-expressing constitutively active PI3K (p110-CAAX), the PH domain of Akt1 (PIP_3 biosensor, PH_{Akt1}), and YFP–GSK3β or YFP–GSK3β^{S9A} were treated with LY29 or LMB (Fig. 2C–E). Interestingly, both YFP–GSK3β and YFP–GSK3β^{S9A} were translocated to the nucleus by LY29, indicating that PI3K signaling regulates GSK3β translocation and that the phosphorylation of GSK3β at Ser9 is not essential for this translocation (Fig. 2C,D and supplementary material Movies 2 and 3).

We then confirmed our results using the opposite approach. After serum deprivation, PI3K signaling was inactivated (supplementary material Fig. S4A). Under these conditions, GSK3β

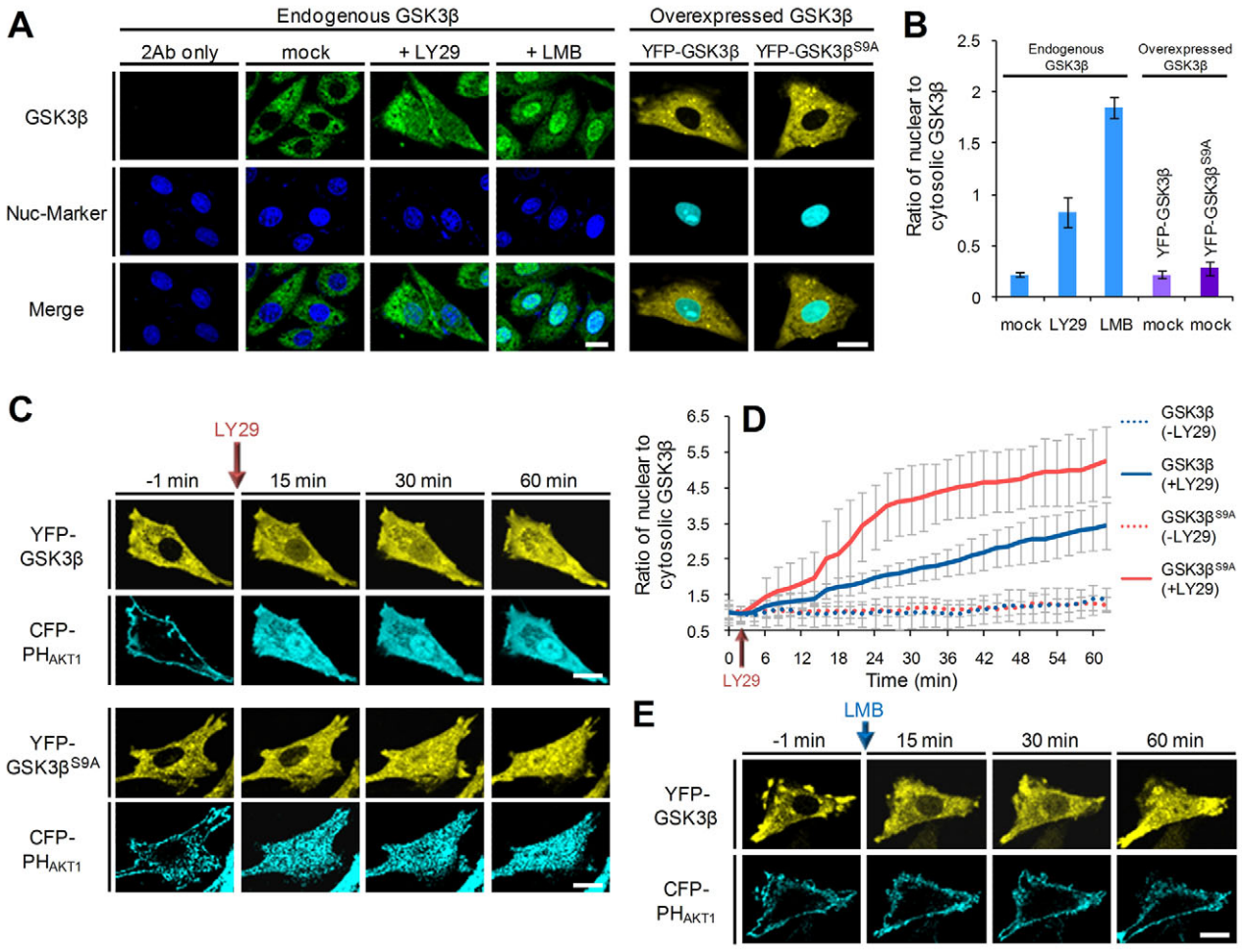

Fig. 2. PI3K promotes the nuclear export of GSK-3β. (**A**) Endogenous GSK3β is localized to the cytosol and translocated to the nucleus after LY29 or LMB treatment for 1 hour. Overexpressed YFP–GSK3β and YFP–GSK3β^{S9A} are localized to the cytosol. Scale bars: 20 µm. (**B**) Quantification of the ratio of nuclear to cytosolic GSK3β shown in A (n=10, error bars indicate s.d.). (**C**) After serum deprivation for 6 hours, the cells coexpressing p110-CAAX with YFP–GSK3β or YFP–GSK3β^{S9A} were treated with LY29 (50 µM). YFP–GSK3β and YFP–GSK3β^{S9A} are translocated to the nucleus following inhibition of PI3K. CFP–PH_{AKT1} was used for monitoring PI3K activity. Scale bar: 20 µm. (**D**) Quantitative measurement of GSK3β and GSK3β^{S9A} translocation after LY29 treatment (n=5, error bars indicate s.d.). (**E**) YFP–GSK3β is translocated to the nucleus following treatment with LMB (25 ng/ml). Scale bar: 20 µm.

was distributed evenly throughout the cells and nuclear GSK3β was exported following treatment with PDGF, a well-known PI3K activator (supplementary material Fig. S4B,C). After preincubation with LY29 for 1 hour, overexpressed YFP–GSK3β or YFP–GSK3β^{S9A} were evenly distributed in the cells coexpressing p110-CAAX and PH_{Akt1}. After LY29 wash out, nuclear YFP–GSK3β and YFP–GSK3β^{S9A} were translocated to the cytosol (supplementary material Fig. S4D), confirming that export of nuclear GSK3β is mediated by PI3K signaling.

The functional role of RCAN1 changes in a dose-dependent manner

To quantitatively analyze the effect of various hypertrophic stimulants on the calcineurin–NFAT signaling network, we simulated nuclear NFAT induction levels, phosphorylated ERK levels and cytosolic GSK3β levels after treatment with AngII, PE, ET-1, PDGF and ISO, respectively. Nuclear NFAT levels were increased prominently following PDGF and AngII treatment (Fig. 3A), and phosphorylated ERK levels were markedly increased by PDGF treatment. Cytosolic GSK3β levels were increased remarkably by AngII, PE and ISO treatment. It can be seen, however, that PE failed to increase phosphorylated ERK levels, and that ET-1 did not increase cytosolic GSK3β levels, which is related to the low level of induction of nuclear NFAT by PE and ET-1. Taken together, these results suggest that the two crosstalk signal pathways mediated by ERK and GSK3β are simultaneously required for full activation of calcineurin–NFAT signaling.

In this model, the calcineurin–NFAT signaling pathway and the RCAN1 regulation module together constitute a core circuit of the signaling network that is most important in merging and processing the hypertrophic signals mediated by cytosolic Ca^{2+} levels and the ERK and PI3K pathways. Thus, our analysis focuses on the functional role of signaling components of the core circuit in manipulation of responses to hypertrophic stimulants. We have simulated the output profiles of phosphorylated RCAN1 (at Ser108) and nuclear NFAT by changing the kinetic parameter values over

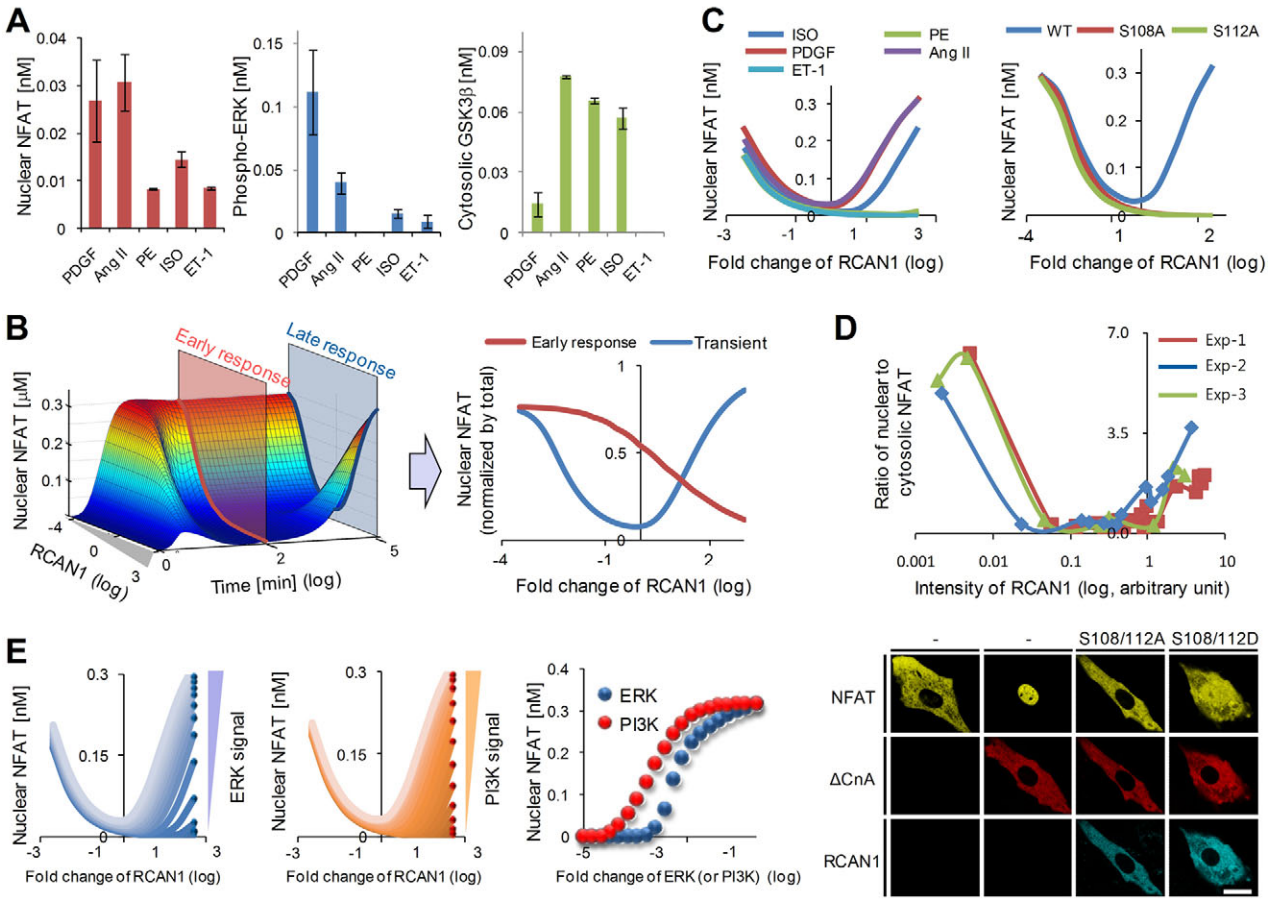

Fig. 3. Dose-dependent role change of RCAN1. (**A**) Nuclear NFAT levels are significantly increased following treatment with PDGF or AngII. PE and ET-1 fail to increase levels of phosphorylated ERK and cytosolic GSK3β, respectively (n=100, error bars indicate s.d.). (**B**) The temporal concentration profiles of nuclear NFAT with respect to the fold increase of RCAN1 after AngII treatment (left). Comparison of the early and late responses of nuclear NFAT (right). (**C**) The biphasic responses of nuclear NFAT are observed only for the PDGF, AngII and ISO stimulations, and not for the PE and ET-1 stimulations (left) and the biphasic phenomena were eliminated following site mutation of Ser112 or Ser108 of RCAN1 (right). (**D**) The ratio of nuclear to cytosolic NFAT depends on RCAN1 intensity (top). $(F_R–F_{BG})/(F_{Ref}–F_{BG})$ where F denotes fluorescent intensity (F_R, RCAN1; F_{BG}, background; F_{Ref}, reference). The live Hoechst 33342 staining was used as a reference (F_{Ref}). All the data were measured within 30 minutes of IM treatment (n=3) (see supplementary material Fig. S7 for representative images and raw data). Nuclear NFAT induced by ΔCnA is inhibited by RCAN1$^{S108/112A}$ and facilitated by RCAN1$^{S108/112D}$ (bottom). This implies that both ERK and GSK3β are simultaneously required to induce the biphasic response of the nuclear NFAT. Scale bar: 20 μm. (**E**) Comparison of the relative effects of two crosstalk signals, mediated by ERK and PI3K, respectively, on induction of nuclear NFAT. A,B,C,E show the simulation results where A,C,E are the steady-state responses after treatment of hypertrophic stimulants.

a wide range. Of the 19 total kinetic parameters, eight parameters (P7–P10, P12–P14 and P19) showed nonlinear ('curved') steady-state trajectories of the outputs in the phase plane (supplementary material Fig. S5). In particular, the fold increase of the four parameters (P7–P10) related to RCAN1 production induced a biphasic response in nuclear NFAT induction (supplementary material Fig. S6), which suggests that depending on its expression level, RCAN1 might have different roles in the regulation of calcineurin–NFAT signaling.

To further investigate the functional role of RCAN1, we simulated the temporal concentration profiles of nuclear NFAT relative to the fold increase of RCAN1. The early responses (within about 200 minutes) of nuclear NFAT after AngII treatment showed a monotonic decrease, but the late responses showed a biphasic curve where the nuclear NFAT increases beyond a certain threshold level of RCAN1 (Fig. 3B). These results further suggest that the role of RCAN1 changes in a dose-dependent manner. To examine whether other hypertrophic stimulants also generate the same result, we simulated the induction levels of nuclear NFAT by gradually increasing the concentration of PE, PDGF, ISO and ET-1, respectively. Under these conditions, the biphasic response of nuclear NFAT was observed only after stimulation with PDGF or ISO, and not after stimulation with PE or ET-1 (Fig. 3C, left). Together with the preceding result indicating that full activation of nuclear NFAT requires crosstalk signals from both ERK and GSK3β (Fig. 3A), this suggests that such crosstalk signals are also related to the induction of the biphasic response of nuclear NFAT. To investigate this possibility, we simulated the nuclear NFAT level changes after site mutation at Ser112 (phosphorylated by ERK) and at Ser108 (phosphorylated by GSK3β), respectively. Site mutation of RCAN1 at Ser112 or Ser108 abolished the increase in nuclear NFAT levels observed at high RCAN1 concentrations (Fig. 3C, right).

To confirm the biphasic response of the nuclear NFAT, we transfected RCAN1 transiently and measured the expression level of RCAN1 through the intensity of CFP-conjugated RCAN1. Hoechst 33342 (nucleus staining in live cells) was used for normalization. The cells expressing NFAT–YFP and RCAN1 were randomly selected and tracked for 30 minutes after ionomycin treatment. NFAT was clearly translocated to the nucleus in the cells that do not express RCAN1 but the NFAT translocation was blocked in the cells that weakly express RCAN1 after ionomycin treatment. However, the cells that highly express RCAN1 showed the nuclear localization of NFAT after ionomycin treatment (upper panel of Fig. 3D and supplementary material Fig. S7). To ensure consistency of simulations under steady-state conditions, we measured the nuclear NFAT level for 30 minutes after ionomycin treatment (we confirmed that the time trajectories of the nuclear NFAT were stabilized after 30 minutes of ionomycin treatment). We found that the experimental results are consistent with the simulation results shown in Fig. 3C, which confirms the biphasic response of the nuclear NFAT. To validate the crosstalk effect from ERK and GSK3β, we investigated the induction of the nuclear NFAT by a point mutation of RCAN1. The nuclear NFAT level was prominently increased in the cells expressing NFATc1–YFP and constitutively active calcineurin (ΔCnA) as shown in Fig. 3D (bottom panel). However, when the cells were further co-transfected with CFP–RCAN1$^{S108/112A}$ in which both ERK and GSK3β phosphorylation sites were mutated to Ala, nuclear NFAT was exported to the cytosol. This is consistent with the simulation result (Fig. 3C, right). To confirm the facilitative role of RCAN1 in the nuclear NFAT induction, we further co-transfected the cells with CFP–RCAN1$^{S108/112D}$ in which both ERK and GSK3β phosphorylation sites were mutated to Asp. A large amount, if not all, of the cytosolic NFAT was imported to the nucleus (note that such a mutation effect is always less prominent than biochemical phosphorylation). To further confirm the facilitative mechanism of RCAN1 using hypertrophic ligands, we increased the expression level of RCAN1 through incubation of cells with ionomycin for 1 hour (we confirmed that RCAN1 expression level was elevated within 30 minutes and sustained for 1 hour). After ionomycin was washed out, the cells were treated with PDGF and NE, respectively. The nuclear NFAT levels were increased in cells treated with PDGF, but not in the cells treated with NE (supplementary material Fig. S8). This is because PDGF effectively activates ERK and cytosolic GSK3β whereas NE activates only GSKβ, as shown in Fig. 3A. Taken together with the simulation results (Fig. 3C, right), these suggest that both ERK and GSK3β are simultaneously required to induce the biphasic response of the nuclear NFAT.

To compare the relative effects of these two crosstalk signals, we further investigated the induction levels of nuclear NFAT relative to the fold change of RCAN1 for each crosstalk signal (Fig. 3E). The nuclear NFAT levels for a fixed high concentration of RCAN1 increased along with the fold increase of ERK or PI3K, but the threshold at which nuclear NFAT levels started to increase was much higher for ERK than for PI3K. Such different threshold levels might arise because of the distinct roles of ERK and PI3K in calcineurin–NFAT signaling: ERK re-establishes calcineurin activity by releasing RCAN1 from the calcineurin complex, whereas GSK3β exported to the cytosol by PI3K directly facilitates calcineurin–NFAT signaling in cooperation with 14-3-3 (Abbasi et al., 2006).

The incoherent regulation switch coordinates the role change of RCAN1

In the above sections, the functional role of RCAN1 was found to switch from inhibition to facilitation of calcineurin–NFAT signaling in a dose-dependent manner. The question then arises as to whether there is a core circuit in the calcineurin–NFAT signaling network that coordinates such a role change of RCAN1. To answer this question, we further simplified the signaling network model by considering only three major signaling proteins that are directly related to RCAN1: calcineurin, NFAT and RCAN1. In this simplified model, we assumed that the crosstalk signals mediated through ERK and GSK3β are constitutively active and that there is no transcriptional time delay for RCAN1 (supplementary material Table S4). To validate whether the response profiles of the simplified model are similar enough to those of the full model, we compared the response curves of the nuclear NFAT and the active calcineurin along with the gradual increase of RCAN1 and confirmed that the simplified model represents the dynamic behavior of the full model in a consistent way (supplementary material Fig. S9). By dissecting this simplified model, we identified a central incoherent regulation circuit where the nonphosphorylated RCAN1 binds to calcineurin and inhibits its activity (negative regulation), whereas the sequentially phosphorylated RCAN1 facilitates calcineurin–NFAT signaling (positive regulation), as shown on the left in Fig. 4A. This incoherent regulation circuit conceptually functions as a regulation switch in which the crosstalk signals mediated through ERK and GSK3β divert the negative regulation by RCAN1 to a positive regulation (Fig. 4A, right). The incoherent regulation switch is structurally similar to the incoherent feed-forward loop that is widely known to induce a biphasic response (Kim et al., 2008; Mangan et al., 2006). This provides us

with a hint on the hidden regulatory mechanism underlying the role change of RCAN1 in calcineurin–NFAT signaling.

The next question that arises concerns which particular molecular interactions dominantly contribute to the induction of the biphasic response of nuclear NFAT. To address this question, we generated 10,000 sets of random parameter values selected from a log-uniform distribution over a range of the order of 10^2 and simulated the corresponding profiles of the nuclear NFAT activity with respect to the fold increase of RCAN1 (supplementary material Table S4). These profiles were then clustered into two groups: 'monotonic increase' and 'concave-up'. By comparing the parameter values of these two profile groups, we found that the sequential phosphorylation of RCAN1 (k6 and k7) and the inhibition of calcineurin by RCAN1 binding (k3) primarily contribute to induction of the biphasic response (Fig. 4B). Taken together, these results show that the biphasic response of the nuclear NFAT is implemented via an intricate balance between the positive and negative regulation pathways in the core regulation switch.

Discussion

The functional role of RCAN1 has been under debate since it became clear that its function changes depending on experimental conditions. In this study, we have unraveled the mechanisms and principles underlying regulation by RCAN1 using a combined approach of single-cell experimentation and in silico simulations. In particular, we revealed that PI3K signaling prompts the nuclear export of GSK3β, a translocation mechanism that had been unclear in cardiac cells. Based on this, together with integrated information from previous experiments, we developed a mathematical model of the calcineurin–NFAT signaling network. Through extensive in silico simulations using this model, we found that RCAN1 has different roles in a dose-dependent manner: as an inhibitor of calcineurin–NFAT signaling when RCAN1 levels are low, and as a facilitator when RCAN1 levels are high. Furthermore, we have identified an incoherent regulation switch that coordinates this role change of RCAN1.

Our finding that a gradual increase in RCAN1 levels induces a biphasic response ('concave-up') of nuclear NFAT elucidates why the role of RCAN1 changes under different experimental conditions. Let us consider the case in which the induction level of RCAN1 lies below a critical value (*Rc*) under a certain set of biological conditions (Fig. 4C, left). In this case, nuclear NFAT levels would decrease along with the increase in RCAN1. If RCAN1 levels were suddenly reduced using knockout methods, nuclear NFAT levels would increase, leading to the interpretation that RCAN1 is inhibitory under this condition. However, if RCAN1 levels were strongly increased over the critical value (RCAN1>>*Rc*) using overexpression methods, nuclear NFAT contents would also be increased, leading to the interpretation that RCAN1 is a facilitator of NFAT levels under this condition (Fig. 4C, left). If the initial induction level of RCAN1 were already beyond the critical value, nuclear NFAT levels would increase along with those of RCAN1 (Fig. 4C, middle). In this case, nuclear NFAT levels would decrease or increase in knockout or overexpression models of RCAN1, suggesting that RCAN1 has a consistent role in facilitating NFAT levels. However, if the crosstalk signals mediated by ERK and GSK3β were absent, the biphasic response of nuclear NFAT would disappear, and nuclear NFAT levels would monotonically decrease along with those of RCAN1, suggesting an inhibitory role of RCAN1 (Fig. 4C, right).

Up to now, many attempts have been made to explain the contentious role of RCAN1 in calcineurin–NFAT signaling. For instance, Molkentin and colleagues reported that TAK1 phosphorylates RCAN1 at Ser94 and Ser136, and that this converts RCAN1 from an inhibitor to a facilitator of calcineurin–NFAT signaling (Liu et al., 2009); however, the molecular mechanisms

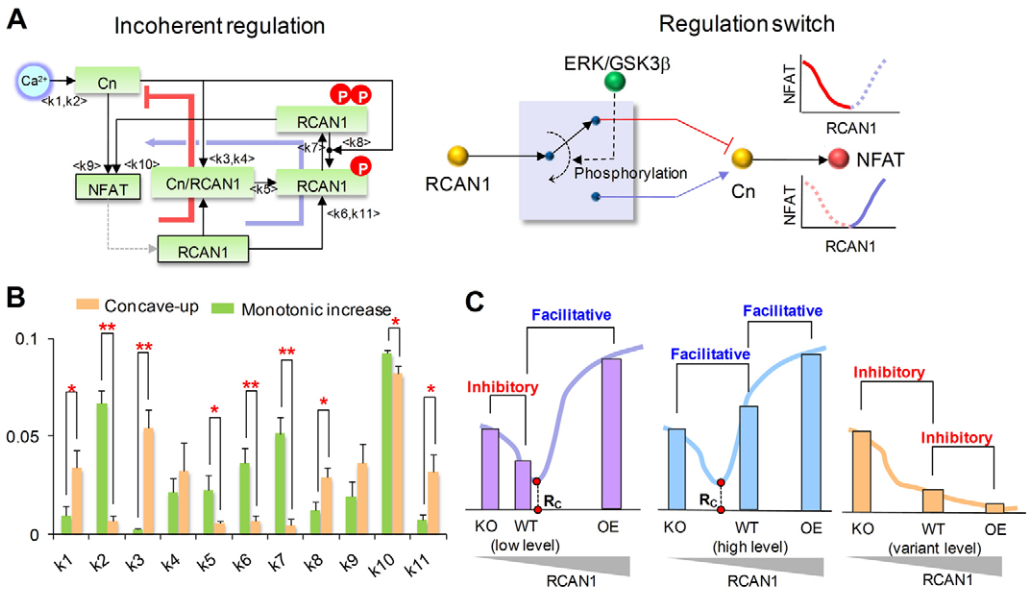

Fig. 4. An incoherent regulation switch coordinates the role change of RCAN1. (**A**) The inherent regulation circuit, where nonphosphorylated RCAN1 binds to calcineurin and inhibits calcineurin activity (negative regulation), whereas the sequentially phosphorylated RCAN1 facilitates calcineurin–NFAT signaling (positive regulation) (left). This incoherent regulation circuit conceptually functions as a regulation switch in which the crosstalk signals mediated through ERK and GSK3β divert the negative regulation by RCAN1 to a positive regulation (right). (**B**) Comparison of the parameter values of two profile groups ('concave-up' and 'monotonic increase') (error bars indicate s.d.; **P*<0.05 and ***P*<0.01). (**C**) The biphasic response of NFAT ('concave-up') to a gradual increase in RCAN1 levels explains why different roles for RCAN1 have been proposed under various experiments.

responsible for this facilitation were not fully addressed. Kishi and co-workers reported that phosphorylation of yeast RCAN1 (Rcn1) triggers its degradation through the SCF^{Cdc4} ubiquitin ligase complex, which mitigates inhibition of calcineurin by Rcn1 (Tokudome et al., 2005). Cunningham and colleagues reported through structure–function analysis that the inhibitory effect of RCAN1 requires a degenerate PxIxIT-like motif and an LxxP motif, whereas its facilitatory effect requires a TxxP motif, an ExxP motif, the GSK3β phosphorylation site SCF^{Cdc4}, and the proteasome (Mehta et al., 2009). In this study, we have shown that the change in the role of RCAN1 is coordinated by the incoherent regulation switch of the calcineurin–NFAT signaling network. However, the detailed mechanism by which calcineurin–NFAT signaling is facilitated after phosphorylation of RCAN1 by GSK3β remains unclear. In the mathematical model, we highlighted only the fact that the sequentially phosphorylated RCAN1 directly contributes to calcineurin dephosphorylation of NFAT, as reported in a previous experiment (Abbasi et al., 2006). By contrast, other authors (Mehta et al., 2009; Tokudome et al., 2005) suggested that calcineurin–NFAT signaling increases through degradation of RCAN1 by SCF^{Cdc4} ubiquitin ligase after GSK3β phosphorylation of RCAN1. However, this can explain only the re-establishment (‘restoration’) of calcineurin–NFAT signaling and not the facilitation (‘increase’). In addressing this problem, we might consider the 14-3-3 protein, which has been reported to bind to over 200 substrates including NFAT, and also to recognize specifically the phosphoserine/threonine-containing sequence motifs in target proteins (Liao et al., 2005). In particular, 14-3-3 inhibits the nuclear import of NFAT by binding to phosphorylated NFAT (Chow and Davis, 2000; Liao et al., 2005). Phosphorylated RCAN1 is another target substrate of 14-3-3, and therefore, if phosphorylated RCAN1 levels dramatically increase, the levels of the complex of NFAT and 14-3-3 would also decrease. This means that highly increased phosphorylated RCAN1 levels might result in competitive inhibition of the binding between NFAT and 14-3-3, which would lead to facilitation of the nuclear import of NFAT. This hypothesis could explain the facilitative role of RCAN1 when its levels are high, as shown in our simulations.

The incoherent regulation switch that coordinates the role change of RCAN1 is structurally similar to the incoherent feed-forward loop, which is one of the most common network motifs in transcription regulatory networks and protein-protein interaction networks (Kim et al., 2008; Mangan and Alon, 2003). This network motif is known to induce a fast activation followed by a delayed inhibition of the output response to a given input stimulation (Mangan and Alon, 2003), and thereby results in time-dependent biphasic responses (Kim et al., 2008). The incoherent feed-forward regulation can also induce dose-dependent biphasic responses (Kim et al., 2008), and such response profiles can be further shaped as either ‘concave-up’ or ‘concave-down’ depending on the intricate balance between the negative and positive regulations that comprise the incoherent feed-forward circuit. For instance, if the positive regulation is stronger than the negative regulation for a low-level stimulation, then a concave-down-shaped curve will be generated; otherwise, a concave-up-shaped curve will be generated. In this study, we found that the incoherent regulation switch can also generate such a biphasic response. This means that a biological system containing an incoherent regulation switch can induce apparently opposite responses depending on biological conditions, which explains why different roles of RCAN1 in calcineurin–NFAT signaling have been suggested under various experimental conditions.

Materials and Methods

Materials

Endothelin-1 was purchased from the Peptide Institute, PDGF-BB was purchased from PeproTech and leptomycin B and norepinephrine were purchased from Sigma. Ionomycin (Sigma), LY294002 (LC Laboratories) and U0126 (Promega) were dissolved in dimethyl sulphoxide (DMSO; Sigma) and used at the indicated concentrations.

Plasmids

GSK3β and $GSK3β^{S9A}$ were generated using RT-PCR cloning with gene-specific primers containing attB sequences to create entry clones for the Gateway cloning system® (Invitrogen). Expression constructs were made using LR clonase (Invitrogen) to transfer the coding regions into YFP expression vectors. The NFATc1–YFP construct was made by exchange of the sequence encoding fluorescent protein of NFATc1–GFP, which was kindly provided by Colleen M. Sheridan (Sheridan et al., 2002). CFP and GFP-PH_{AKT1} were gifts from Tobias Myer (Stanford University, Palo Alto, CA). RCAN1 and truncation of Calcineurin (1–398) were amplified by PCR and subcloned into CFP-C1 and mCherry-C1 vectors (Clontech), respectively. $RCAN1^{S108/112A}$ and $RCAN1^{S108/112D}$ were generated using the QuikChange site-directed mutagenesis kit (Stratagene).

Cell culture and electroporation

H9C2 cells were purchased from the American Type Culture Collection (ATCC). Cells were cultured in Dulbecco’s modified Eagles medium (DMEM; Invitrogen) supplemented with 10% FBS, 2 mM L-glutamine, and penicillin-streptomycin at 37°C in 10% CO_2. Electroporation was performed using a Microporator™ (MP-100; Digital Bio Technology), following the manufacturer’s instructions. For cell imaging, shocked cells were aliquotted into 96-well black plates with glass-bottoms (Metrical) and, after 24 hours, cells were used for imaging.

Imaging and microscopes

Before imaging, the medium was replaced with phosphate-buffered saline (PBS) containing glucose (1 g/l, Invitrogen). All images were taken using a confocal microscope (A1R, Nikon) with a CFI plan Apochromat VC objective lens (60×/1.40 oil) at a resolution of 512×512. Images were analyzed using MetaMorph software (Molecular Devices).

Measurement of cytosolic Ca^{2+} levels

H9C2 cells were incubated with serum-free DMEM containing 1 μM Fluo-4 and AM ester (Invitrogen) at 37°C. Cells were incubated for 1 hour and washed twice with PBS before imaging.

Immunocytochemistry

For analysis of endogenous GSK-3β localization, cells were exposed to LY29 and LMB for 1 hour without serum starvation, or PDGF for 10 minutes with serum starvation for 6 hours, in serum-free DMEM media. Cells were fixed in 4% paraformaldehyde for 15 minutes, rinsed in Dulbecco’s phosphate-buffered saline solution (DPBS; Invitrogen), permeabilized in ice-cold 100% methanol for 10 minutes, rinsed three times in DPBS, and blocked in DPBS containing 0.3% Triton X-100 (Sigma) and 5% fetal bovine serum (FBS) for 1 hour at room temperature. Primary antibody solutions were made up at a 1:100 dilution in DPBS containing 0.3% Triton X-100, and cells were incubated overnight at 4°C. Cells were rinsed three times for 5 minutes each in DPBS, and then incubated for 1 hour at room temperature in the appropriate secondary antibody at a 1:1000 dilution in blocking solution. After washing three times in DPBS for 5 minutes per wash, cells were incubated briefly in 4′-6-diamidino-2-phenylindole (DAPI; Invitrogen). Fixed cells were stored at 4°C for up to 1 week. Primary antibodies were anti-GSK3β (BD Transduction Laboratories) and anti-phosphorylated GSK3β (Ser9, Cell Signaling Technology). Alexa Fluor secondary antibodies from Molecular Probes were used in all cases.

RNA extraction and real-time quantitative PCR

After harvesting trypsinized H9C2 cells, total RNA was extracted using an easy-BLUE RNA extraction kit (iNtRON) and complementary DNA was synthesized with a cDNA synthesis kit (Invitrogen). Real-time quantitative PCR was performed using the IQ5 real-time PCR detection system (BioRad) with 2× prime Q-master mix (Genet Bio, dye SybrGreen I). The primers used were (5′→3′) RCAN forward, GCCCAATCCAGACAAACAGT and reverse, TCCTCTTCCTCCTCCTCCTC; and internal control GAPDH forward, CTCATGACCACAGTCCATGC and reverse, TTCAGCTCTGGGATGACCTT. PCR product quality was monitored with post-PCR melt curve analysis. Fold inductions were calculated using the comparative Ct (cycle threshold) method (also known as ΔΔCt method) (Livak and Schmittgen, 2001).

Mathematical modeling and analysis

The ordinary differential equations for the mathematical model of the calcineurin–NFAT signaling network and the simplified model are presented in supplementary material Tables S1–S4. The numerical integration was performed using Matlab R2009a software. The kinetic parameters were fitted to the previous experimental

data as well as to our own experimental data obtained from H9C2 cells. The parameter estimates are summarized in supplementary material Tables S5–S7. To examine the robustness of our mathematical model to parameter variations, we carried out extensive simulations repetitively (n=50) over 50% random variation of parameter values selected from a log-uniform distribution and confirmed that the responses of the nuclear NFAT and the active calcineurin of the full and simplified models with respect to the gradual increase of RCAN1 are well preserved to such parameter variations (supplementary material Fig. S9).

The authors are grateful to Ki-Sun Kwon for providing the GSK3β and GSK3β^{S9A} constructs, and thank Je-Hoon Song for helpful discussion. This work was supported by the National Research Foundation of Korea (NRF) grants funded by the Korea Government, the Ministry of Education, Science & Technology (MEST) (2009-0086964, 2010-0017662, 2010-0002160 and 2010-0000617).

Supplementary material available online at
http://jcs.biologists.org/cgi/content/full/124/1/82/DC1

References

Abbasi, S., Su, B., Kellems, R. E., Yang, J. and Xia, Y. (2005). The essential role of MEKK3 signaling in angiotensin II-induced calcineurin/nuclear factor of activated T-cells activation. *J. Biol. Chem.* **280**, 36737-36746.

Abbasi, S., Lee, J. D., Su, B., Chen, X., Alcon, J. L., Yang, J., Kellems, R. E. and Xia, Y. (2006). Protein kinase-mediated regulation of calcineurin through the phosphorylation of modulatory calcineurin-interacting protein 1. *J. Biol. Chem.* **281**, 7717-7726.

Aoki, H., Richmond, M., Izumo, S. and Sadoshima, J. (2000). Specific role of the extracellular signal-regulated kinase pathway in angiotensin II-induced cardiac hypertrophy in vitro. *Biochem. J.* **347**, 275-284.

Baek, K. H., Zaslavsky, A., Lynch, R. C., Britt, C., Okada, Y., Siarey, R. J., Lensch, M. W., Park, I. H., Yoon, S. S., Minami, T. et al. (2009). Down's syndrome suppression of tumour growth and the role of the calcineurin inhibitor DSCR1. *Nature* **459**, 1126-1130.

Chan, B., Greenan, G., McKeon, F. and Ellenberger, T. (2005). Identification of a peptide fragment of DSCR1 that competitively inhibits calcineurin activity in vitro and in vivo. *Proc. Natl. Acad. Sci. USA* **102**, 13075-13080.

Chow, C. W. and Davis, R. J. (2000). Integration of calcium and cyclic AMP signaling pathways by 14-3-3. *Mol. Cell. Biol.* **20**, 702-712.

Clerk, A., Aggeli, I. K., Stathopoulou, K. and Sugden, P. H. (2006). Peptide growth factors signal differentially through protein kinase C to extracellular signal-regulated kinases in neonatal cardiomyocytes. *Cell. Signal.* **18**, 225-235.

Dey, A., Hill, J. A. and Rothermel, B. A. (2007). A cullin 4a E3 ligase complex mediates rapid degradation of the calcineurin regulatory protein MCIP1.4 in cardiac myocytes. *Circulation* **116**, II_305.

Du, J., Liao, W., Wang, Y., Han, C. and Zhang, Y. (2005). Inhibitory effect of 14-3-3 proteins on serum-induced proliferation of cardiac fibroblasts. *Eur. J. Cell Biol.* **84**, 843-852.

Fox, D. S. and Heitman, J. (2005). Calcineurin-binding protein Cbp1 directs the specificity of calcineurin-dependent hyphal elongation during mating in Cryptococcus neoformans. *Eukaryotic Cell* **4**, 1526-1538.

Franca-Koh, J., Yeo, M., Fraser, E., Young, N. and Dale, T. C. (2002). The regulation of glycogen synthase kinase-3 nuclear export by Frat/GBP. *J. Biol. Chem.* **277**, 43844-43848.

Haq, S., Choukroun, G., Kang, Z. B., Ranu, H., Matsui, T., Rosenzweig, A., Molkentin, J. D., Alessandrini, A., Woodgett, J., Hajjar, R. et al. (2000). Glycogen synthase kinase-3beta is a negative regulator of cardiomyocyte hypertrophy. *J. Cell Biol.* **151**, 117-130.

Hilioti, Z., Gallagher, D. A., Low-Nam, S. T., Ramaswamy, P., Gajer, P., Kingsbury, T. J., Birchwood, C. J., Levchenko, A. and Cunningham, K. W. (2004). GSK-3 kinases enhance calcineurin signaling by phosphorylation of RCNs. *Genes Dev.* **18**, 35-47.

Hill, J. A., Rothermel, B., Yoo, K. D., Cabuay, B., Demetroulis, E., Weiss, R. M., Kutschke, W., Bassel-Duby, R. and Williams, R. S. (2002). Targeted inhibition of calcineurin in pressure-overload cardiac hypertrophy. Preservation of systolic function. *J. Biol. Chem.* **277**, 10251-10255.

Hoeffer, C. A., Dey, A., Sachan, N., Wong, H., Patterson, R. J., Shelton, J. M., Richardson, J. A., Klann, E. and Rothermel, B. A. (2007). The Down syndrome critical region protein RCAN1 regulates long-term potentiation and memory via inhibition of phosphatase signaling. *J. Neurosci.* **27**, 13161-13172.

Kim, D., Kwon, Y. K. and Cho, K. H. (2008). The biphasic behavior of incoherent feed-forward loops in biomolecular regulatory networks. *BioEssays* **30**, 1204-1211.

Kruger, M., Sachse, C., Zimmermann, W. H., Eschenhagen, T., Klede, S. and Linke, W. A. (2008). Thyroid hormone regulates developmental titin isoform transitions via the phosphatidylinositol-3-kinase/AKT pathway. *Circ. Res.* **102**, 439-447.

Liang, Q., Bueno, O. F., Wilkins, B. J., Kuan, C. Y., Xia, Y. and Molkentin, J. D. (2003). c-Jun N-terminal kinases (JNK) antagonize cardiac growth through cross-talk with calcineurin-NFAT signaling. *EMBO J.* **22**, 5079-5089.

Liao, W., Wang, S., Han, C. and Zhang, Y. (2005). 14-3-3 proteins regulate glycogen synthase 3beta phosphorylation and inhibit cardiomyocyte hypertrophy. *FEBS J.* **272**, 1845-1854.

Liu, Q., Busby, J. C. and Molkentin, J. D. (2009). Interaction between TAK1-TAB1-TAB2 and RCAN1-calcineurin defines a signalling nodal control point. *Nat. Cell Biol.* **11**, 154-161.

Livak, K. J. and Schmittgen, T. D. (2001). Analysis of relative gene expression data using real-time quantitative PCR and the 2(-Δ Δ C(T)) method. *Methods* **25**, 402-408.

Mangan, S. and Alon, U. (2003). Structure and function of the feed-forward loop network motif. *Proc. Natl. Acad. Sci. USA* **100**, 11980-11985.

Mangan, S., Itzkovitz, S., Zaslaver, A. and Alon, U. (2006). The incoherent feed-forward loop accelerates the response-time of the gal system of Escherichia coli. *J. Mol. Biol.* **356**, 1073-1081.

Markou, T., Cullingford, T. E., Giraldo, A., Weiss, S. C., Alsafi, A., Fuller, S. J., Clerk, A. and Sugden, P. H. (2008). Glycogen synthase kinases 3alpha and 3beta in cardiac myocytes: regulation and consequences of their inhibition. *Cell Signal.* **20**, 206-218.

Mehta, S., Li, H., Hogan, P. G. and Cunningham, K. W. (2009). Domain architecture of the regulators of calcineurin (RCANs) and identification of a divergent RCAN in yeast. *Mol. Cell. Biol.* **29**, 2777-2793.

Minami, T., Horiuchi, K., Miura, M., Abid, M. R., Takabe, W., Noguchi, N., Kohro, T., Ge, X., Aburatani, H., Hamakubo, T. et al. (2004). Vascular endothelial growth factor- and thrombin-induced termination factor, down syndrome critical region-1, attenuates endothelial cell proliferation and angiogenesis. *J. Biol. Chem.* **279**, 50537-50554.

Morisco, C., Zebrowski, D., Condorelli, G., Tsichlis, P., Vatner, S. F. and Sadoshima, J. (2000). The Akt-glycogen synthase kinase 3beta pathway regulates transcription of atrial natriuretic factor induced by beta-adrenergic receptor stimulation in cardiac myocytes. *J. Biol. Chem.* **275**, 14466-14475.

Morisco, C., Seta, K., Hardt, S. E., Lee, Y., Vatner, S. F. and Sadoshima, J. (2001). Glycogen synthase kinase 3beta regulates GATA4 in cardiac myocytes. *J. Biol. Chem.* **276**, 28586-28597.

Morisco, C., Marrone, C., Galeotti, J., Shao, D., Vatner, D. E., Vatner, S. F. and Sadoshima, J. (2008). Endocytosis machinery is required for beta1-adrenergic receptor-induced hypertrophy in neonatal rat cardiac myocytes. *Cardiovasc. Res.* **78**, 36-44.

Morris, J. B., Kenney, B., Huynh, H. and Woodcock, E. A. (2005). Regulation of the proapoptotic factor FOXO1 (FKHR) in cardiomyocytes by growth factors and alpha1-adrenergic agonists. *Endocrinology* **146**, 4370-4376.

Rusnak, F. and Mertz, P. (2000). Calcineurin: form and function. *Physiol. Rev.* **80**, 1483-1521.

Ryeom, S., Greenwald, R. J., Sharpe, A. H. and McKeon, F. (2003). The threshold pattern of calcineurin-dependent gene expression is altered by loss of the endogenous inhibitor calcipressin. *Nat. Immunol.* **4**, 874-881.

Sanna, B., Brandt, E. B., Kaiser, R. A., Pfluger, P., Witt, S. A., Kimball, T. R., van Rooij, E., De Windt, L. J., Rothenberg, M. E., Tschop, M. H. et al. (2006). Modulatory calcineurin-interacting proteins 1 and 2 function as calcineurin facilitators in vivo. *Proc. Natl. Acad. Sci. USA* **103**, 7327-7332.

Sheridan, C. M., Heist, E. K., Beals, C. R., Crabtree, G. R. and Gardner, P. (2002). Protein kinase A negatively modulates the nuclear accumulation of NF-ATc1 by priming for subsequent phosphorylation by glycogen synthase kinase-3. *J. Biol. Chem.* **277**, 48664-48676.

Shin, S. Y., Choo, S. M., Kim, D., Baek, S. J., Wolkenhauer, O. and Cho, K. H. (2006). Switching feedback mechanisms realize the dual role of MCIP in the regulation of calcineurin activity. *FEBS Lett.* **580**, 5965-5973.

Shin, S. Y., Yang, J. M., Choo, S. M., Kwon, K. S. and Cho, K. H. (2008). System-level investigation into the regulatory mechanism of the calcineurin/NFAT signaling pathway. *Cell. Signal.* **20**, 1117-1124.

Tian, B., Liu, J., Bitterman, P. and Bache, R. J. (2003). Angiotensin II modulates nitric oxide-induced cardiac fibroblast apoptosis by activation of AKT/PKB. *Am. J. Physiol. Heart Circ. Physiol.* **285**, H1105-H1112.

Tokudome, T., Horio, T., Fukunaga, M., Okumura, H., Hino, J., Mori, K., Yoshihara, F., Suga, S., Kawano, Y., Kohno, M. et al. (2004). Ventricular nonmyocytes inhibit doxorubicin-induced myocyte apoptosis: involvement of endogenous endothelin-1 as a paracrine factor. *Endocrinology* **145**, 2458-2466.

Tokudome, T., Horio, T., Kishimoto, I., Soeki, T., Mori, K., Kawano, Y., Kohno, M., Garbers, D. L., Nakao, K. and Kangawa, K. (2005). Calcineurin-nuclear factor of activated T cells pathway-dependent cardiac remodeling in mice deficient in guanylyl cyclase A, a receptor for atrial and brain natriuretic peptides. *Circulation* **111**, 3095-3104.

Tomida, T., Hirose, K., Takizawa, A., Shibasaki, F. and Iino, M. (2003). NFAT functions as a working memory of Ca2+ signals in decoding Ca2+ oscillation. *EMBO J.* **22**, 3825-3832.

Vega, R. B., Yang, J., Rothermel, B. A., Bassel-Duby, R. and Williams, R. S. (2002). Multiple domains of MCIP1 contribute to inhibition of calcineurin activity. *J. Biol. Chem.* **277**, 30401-30407.

Vega, R. B., Bassel-Duby, R. and Olson, E. N. (2003a). Control of cardiac growth and function by calcineurin signaling. *J. Biol. Chem.* **278**, 36981-36984.

Vega, R. B., Rothermel, B. A., Weinheimer, C. J., Kovacs, A., Naseem, R. H., Bassel-Duby, R., Williams, R. S. and Olson, E. N. (2003b). Dual roles of modulatory calcineurin-interacting protein 1 in cardiac hypertrophy. *Proc. Natl. Acad. Sci. USA* **100**, 669-674.

Yin, F., Wang, Y. Y., Du, J. H., Li, C., Lu, Z. Z., Han, C. and Zhang, Y. Y. (2006). Noncanonical cAMP pathway and p38 MAPK mediate beta2-adrenergic receptor-induced IL-6 production in neonatal mouse cardiac fibroblasts. *J. Mol. Cell. Cardiol.* **40**, 384-393.

Yook, J. I., Li, X. Y., Ota, I., Hu, C., Kim, H. S., Kim, N. H., Cha, S. Y., Ryu, J. K., Choi, Y. J., Kim, J. et al. (2006). A Wnt-Axin2-GSK3beta cascade regulates Snail1 activity in breast cancer cells. *Nat. Cell Biol.* **8**, 1398-1406.

Table S1. The mathematical model of the calcineurin-NFAT signaling pathway and RCAN1 regulation. Variables are as follows: $[CaCaM]$: Calcium-bound calmodulin, $[Cn^{act}]$: Active form of calcineurin, complex of calcineurin and calcium-bound calmodulin, $[Cn^{occ}]$: RCAN1-occupied calcineurin, complex of the active calcineurin and RCAN1, $[Cn^{off}]$: Free calcineurin to which calcium-bound calmodulin or RCAN1 was not bound, $[NFAT^{in}]$: NFAT in the nucleus, $[NFAT^{out}]$: NFAT in the cytosol, $[Tx_1]$: Non-specified transcription cofactor for RCAN1 expression, $[Tx_2]$: Non-specified transcription cofactor for RCAN1 expression, $[RCAN1^{tot}]$: Total concentration of RCAN1 expressed by NFAT, $[RCAN1^{off}]$: Free RCAN1, non-phosphorylated and non-bound form of RCAN1, $[RCAN1^{S112}]$: RCAN1 phosphorylated at Ser 112 by ERK, $[RCAN1^{S108}]$: RCAN1 phosphorylated at Ser 108 by GSK3β. Initial conditions are as follows: $[CaCaM]$ =0nM, $[Cn^{act}]$ = $[Cn^{occ}]$ =0nM, $[Cn^{off}]$ =2nM, $[NFAT^{in}]$ =0nM, $[NFAT^{out}]$ =0.4 nM, $[Tx_1]=[Tx_2]$=0nM, $[RCAN1^{tot}]$=0nM, $[RCAN1^{off}]$=0nM, $[RCAN1^{S108}]$=0 nM, $[RCAN1^{S112}]$=0nM. The kinetic parameters are defined in Table S5.

$$\frac{d[CaCaM]}{dt} = K_{CaM}^{on}[Ca] - K_{CaM}^{off}[CaCaM]$$

$$\frac{d[Cn^{act}]}{dt} = K_{Cat}^{on}[Cn^{off}][CaCaM] - K_{Cat}^{off}[Cn^{act}] - \frac{d[Cn^{occ}]}{dt}$$

$$\frac{d[Cn^{occ}]}{dt} = K_{MCIP1}^{occ}[Cn^{act}][RCAN1^{off}] - K_{MCIP1}^{rev}[Cn^{occ}] - K_{Cn}^{cat}[Cn^{occ}][ERK^{pp}]$$

$$\frac{d[Cn^{off}]}{dt} = -\frac{d[Cn^{act}]}{dt} - \frac{d[Cn^{occ}]}{dt}$$

$$\frac{d[NFAT^{in}]}{dt} = K_{NFAT}^{in}\left(1 + K_{MCIP1}^{facil}[RCAN1^{S108}]\right)[Cn^{act}][NFAT^{out}] - \left(K_{Export}^{out} + K_{NFAT}^{out}[GSK3^{in}]\right)[NFAT^{in}]$$

$$\frac{d[NFAT^{out}]}{dt} = -\frac{d[NFAT^{in}]}{dt}$$

$$\frac{d[Tx_1]}{dt} = K_{Tx}^{prod}[NFAT^{in}] - K_{Tx}^{deg}[Tx_1]$$

$$\frac{d[Tx_2]}{dt} = K_{Tx}^{prod}[Tx_1] - K_{Tx}^{deg}[Tx_2]$$

$$\frac{d[RCAN1^{tot}]}{dt} = K_{RCAN1}^{prod}[Tx_2] - K_{RCAN1}^{deg}[RCAN1^{tot}]$$

$$\frac{d[RCAN1^{off}]}{dt} = \frac{d[RCAN1^{tot}]}{dt} - \left(\frac{d[RCAN1^{S112}]}{dt} + \frac{d[RCAN1^{S108}]}{dt} + \frac{d[Cn^{occ}]}{dt}\right)$$

$$\frac{d[RCAN1^{S112}]}{dt} = K_{Cn}^{cat}[Cn^{occ}][ERK^{pp}] + K_{RCAN1}^{cat}[RCAN1^{off}][ERK^{pp}] - K_{s112}^{rev}[RCAN1^{S112}] - \frac{d[RCAN1^{S108}]}{dt}$$

$$\frac{d[RCAN1^{S108}]}{dt} = K_{s112}^{cat}[RCAN1^{S112}][GSK3^{out}] - K_{s108}^{rev}[Cn^{act}][RCAN1^{S108}]$$

Table S2. The mathematical model of the PI3K signaling pathway. It has been reported that ET-1 does not activate the PI3K-Akt signaling pathway but it regulates GSK3β through the ERK signaling pathway (Kruger et al., 2008; Markou et al., 2008; Tokudome et al., 2004). Variables are as follows: $[PI3K^{act}]$: Activated PI3K by its upstream signaling, $[AKT^{pp}]$: Phosphorylated Akt by PK3K, an active form of AKT, $[PFK^{act}]$: Non-specific PI3K inhibitor activated by a feedback regulation, $[GSK3^{in}]$: GSK3β in the nucleus, $[GSK3^{out}]$: GSK3β in the cytosol, $[GSK3^{pp}]$: Phosphorylated GSK3β by the active form of Akt, $[GPP^{act}]$: Non-specific phosphatase of GSK3β. Constants are as follows: $[PI3K^{tot}]$: Total concentration of PI3K, $[AKT^{tot}]$: Total concentration of Akt, $[PFK^{tot}]$: Total concentration of PFK, $[GPP^{tot}]$: Total concentration of GPP. Initial conditions are as follows: $[PI3K^{act}] = [AKT^{pp}] = [PFK^{act}] = 0.02$nM; $[GSK3^{in}] = [GSK3^{out}] = 0.05$nM; $[GSK3^{pp}] = 0.02$nM; $[GPP^{act}] = 0$nM. The kinetic parameters are defined in Table S6.

$$\frac{d[PI3K^{act}]}{dt} = \frac{K_{PI3K}^{cat}[Hs(t)]([PI3K^{tot}]-[PI3K^{act}])}{1+\left(\frac{[PFK^{act}]}{K_{inh}^{PFK}}\right)^{hc}} - K_{PI3K}^{rev}[PI3K^{act}]$$

$$\frac{d[AKT^{pp}]}{dt} = K_{AKT}^{cat}\left([AKT^{tot}]-[AKT^{pp}]\right)[PI3K^{act}] - K_{AKT}^{rev}[AKT^{pp}]$$

$$\frac{d[PFK^{act}]}{dt} = K_{PFK}^{cat}\left([PFK^{tot}]-[PFK^{act}]\right)[PI3K^{act}] - K_{PFK}^{rev}[PFK^{act}]$$

$$\frac{d[GSK3^{in}]}{dt} = K_{GSK3}^{in}[GSK3^{out}] - K_{GSK3}^{out}[GSK3^{in}][AKT^{pp}] - K_{GSK3}^{cat}[GSK3^{in}][AKT^{pp}] + K_{GSK3}^{rev}[GPP^{act}][GSK3^{pp}]$$

$$\frac{d[GSK3^{in}]}{dt} = K_{GSK3}^{in}[GSK3^{out}] - K_{GSK3}^{cat}[GSK3^{in}][ERK^{pp}] + K_{GSK3}^{rev}[GPP^{act}][GSK3^{pp}] \text{ (for ET-1)}$$

$$\frac{d[GSK3^{pp}]}{dt} = K_{GSK3}^{cat}[AKT^{pp}]\left([GSK3^{out}]+[GSK3^{in}]\right) - 2K_{GSK3}^{rev}[GPP^{act}][GSK3^{pp}]$$

$$\frac{d[GSK3^{pp}]}{dt} = K_{GSK3}^{cat}[ERK^{pp}]\left([GSK3^{out}]+[GSK3^{in}]\right) - 2K_{GSK3}^{rev}[GPP^{act}][GSK3^{pp}] \text{ (for ET-1)}$$

$$\frac{d[GPP^{act}]}{dt} = K_{GPP}^{cat}\left([GPP^{tot}]-[GPP^{act}]\right)[GSK3^{pp}] - K_{GPP}^{rev}[GPP^{act}]$$

$$\frac{d[GSK3^{out}]}{dt} = -\frac{d[GSK3^{in}]}{dt} - \frac{d[GSK3^{pp}]}{dt}$$

Table S3. The mathematical model of the ERK signaling pathway. Variables are as follows: $[Ras^{GTP}]$: GTP-bound Ras by its upstream signal, an active form of Ras, $[Raf^{act}]$: Active form of Raf by activated Ras, $[MEK^{pp}]$: Phosphorylated MEK by active Raf, an active form of MEK, $[ERK^{pp}]$: Phosphorylated ERK by active MEK, an active form of ERK, $[RKIP^{pp}]$: Phosphorylated RKIP by active ERK, an inhibited form of RKIP. Constants are as follows: $[Ras^{tot}]$: Total concentration of Ras, $[Raf^{tot}]$: Total concentration of Raf, $[MEK^{tot}]$: Total concentration of MEK, $[ERK^{tot}]$: Total concentration of ERK, $[RKIP^{tot}]$: Total concentration of RKIP. Initial conditions are as follows: $[Ras^{GTP}]$ =0.007nM, $[Raf^{act}]$ =0.0024nM, $[MEK^{pp}]$ =0.0072nM, $[ERK^{pp}]$ =0.0014nM, $[RKIP^{pp}]$ =0.0048nM. The kinetic parameters are defined in Table S7.

$$\frac{d[Ras^{GTP}]}{dt} = \frac{K_{Ras}^{cat}[Hs(t)]\left([Ras^{tot}]-[Ras^{GTP}]\right)}{1+\left(\frac{[ERK^{pp}]}{K_{inh}^{ERK}}\right)^3} - K_{Ras}^{rev}[Ras^{GTP}]$$

$$\frac{d[Raf^{act}]}{dt} = K_{Raf}^{cat}\left([Raf^{tot}]-[Raf^{act}]\right)[Ras^{GTP}]-K_{Raf}^{rev}[Raf^{act}]$$

$$\frac{d[MEK^{pp}]}{dt} = \frac{K_{MEK}^{cat}\left([MEK^{tot}]-[MEK^{pp}]\right)[Raf^{act}]}{1+\left(\frac{[RKIP^{tot}]-[RKIP^{pp}]}{K_{inh}^{RKIP}}\right)^3} - K_{MEK}^{rev}[MEK^{pp}]$$

$$\frac{d[ERK^{pp}]}{dt} = K_{ERK}^{cat}\left([ERK^{tot}]-[ERK^{pp}]\right)[MEK^{pp}]-K_{ERK}^{rev}[ERK^{pp}]$$

$$\frac{d[RKIP^{pp}]}{dt} = K_{RKIP}^{cat}\left([RKIP^{tot}]-[RKIP^{pp}]\right)[ERK^{pp}]-K_{RKIP}^{rev}[RKIP^{pp}]$$

Table S4. The simplified mathematical model of the signaling pathway. Variables are as follows: $[Cn]$: Activated calcineurin through calcium binding, $[Co]$: Complex of calcineurin and RCNA1, $[M_1]$: Single phosphorylated RCAN1, $[M_2]$: Double phosphorylated RCAN1, $[NF]$: Nuclear NFAT. In order to simulate the response profiles of the nuclear NFAT activity in the simplified model along with the fold increase of RCAN1, 10,000 sets of random parameter values were selected from a log-uniform distribution over the range between10^{-3} and 10^{-1}.

$$\frac{d[Cn]}{dt} = k_1\left(1-[Cn]-[Co]\right) - k_2[Cn] - \frac{d[Co]}{dt}$$

$$\frac{d[Co]}{dt} = k_3[Cn]\left([M_t]-[M_1]-[M_2]-[Co]\right) - k_4[Co] - k_5[Co]$$

$$\frac{d[M_1]}{dt} = k_5[Co] + k_6\left([M_t]-[M_1]-[M_2]-[Co]\right) - k_{11}[M_1] - k_7[M_1] + k_8[Cn][M_2]$$

$$\frac{d[M_2]}{dt} = k_7[M_1] - k_8[Cn][M_2] - k_d[M_2]$$

$$\frac{d[NF]}{dt} = k_9\left(1+k_{10}[M_2]\right)[Cn]\left(1-[NF]\right) - k_{12}[NF]$$

Table S5. Parameter estimates of the calcineurin-NFAT signaling pathway and RCAN1 regulation module.

Symbol	Unit	Value	Symbol	Unit	Value
K_{Cat}^{on}	$nM^{-1}\ min^{-1}$	1.388E+00	K_{MCIP1}^{occ}	$nM^{-1}\ min^{-1}$	2.873E+00
K_{Cat}^{off}	min^{-1}	1.731E+00	K_{MCIP1}^{rev}	min^{-1}	6.981E-02
K_{NFAT}^{in}	$nM^{-1}\ min^{-1}$	1.191E+00	K_{Cn}^{cat}	$nM^{-1}\ min^{-1}$	1.227E+00
K_{NFAT}^{out}	$nM^{-1}\ min^{-1}$	1.305E-01	K_{MCIP1}^{facil}	nM^{-1}	3.161E-02
K_{CaM}^{on}	$nM\ min^{-1}$	8.760E-02	K_{s112}^{cat}	$nM^{-1}\ min^{-1}$	6.104E-01
K_{CaM}^{off}	min^{-1}	6.732E-01	K_{s108}^{rev}	$nM^{-1}\ min^{-1}$	7.820E-01
K_{Tx}^{prod}	min^{-1}	2.000E-02	K_{MCIP1}^{cat}	$nM^{-1}\ min^{-1}$	6.466E-02
$K_{Tx}^{\deg}$	min^{-1}	2.000E-02	K_{s112}^{rev}	min^{-1}	1.424E-01
K_{MCIP1}^{prod}	min^{-1}	1.000E+03	$NFAT^{tot}$	nM	4.000E-01
K_{MCIP1}^{deg}	min^{-1}	2.000E-01	$GSK3^{tot}$	nM	1.100E-01
K_{Export}^{out}	min^{-1}	6.530E-02	Cn^{tot}	nM	2.000E+00

Table S6. Parameter estimates of the PI3K signaling pathway. We note again that ET-1 does not activate the PI3K-Akt signaling pathway but it regulates GSK3β through the ERK signaling pathways (Kruger et al., 2008; Markou et al., 2008; Tokudome et al., 2004).

Symbol	Unit	ISO	PDGF	AngII	PE	ET-1
K_{PI3K}^{cat}	min^{-1}	1.810E-01	1.201E-01	4.001E-01	4.587E-01	-
K_{PI3K}^{rev}	min^{-1}	6.207E-02	4.847E-01	2.025E+00	4.249E-01	-
K_{AKT}^{cat}	$nM^{-1}\ min^{-1}$	1.017E+00	5.501E-01	1.175E+00	1.721E-01	-
K_{AKT}^{rev}	min^{-1}	7.233E-01	6.765E-01	8.033E-01	1.151E+00	-
K_{PFK}^{cat}	$nM^{-1}\ min^{-1}$	3.898E-01	5.330E-01	9.180E-01	5.522E-01	-
K_{PFK}^{rev}	min^{-1}	8.262E-02	7.244E-03	1.569E-02	2.668E-02	-
$PI3K^{tot}$	nM	2.281E-01	9.837E-01	2.232E-01	7.965E-01	-
AKT^{tot}	nM	4.522E-01	5.163E-01	5.768E-01	3.891E-01	-
PFK^{tot}	nM	1.094E+00	8.793E-01	1.706E+00	1.372E+00	-
K_{inh}^{PFK}	nM	2.379E-02	1.272E-01	4.232E-01	4.664E-01	-
hc	-	1.746E+00	9.632E-01	2.202E+00	2.163E+00	-
K_{GSK3}^{out}	$nM^{-1}\ min^{-1}$	7.946E+00	1.118E+00	5.609E+00	3.085E+00	-
$K_{GSK3out}^{cat}$	$nM^{-1}\ min^{-1}$	1.084E+00	1.584E+00	3.081E+00	4.815E+00	1.255E+00
$K_{GSK3out}^{rev}$	$nM^{-1}\ min^{-1}$	1.150E+00	1.483E-01	1.249E+00	9.748E-01	1.973E+00
K_{GPP}^{cat}	$nM^{-1}\ min^{-1}$	3.218E-01	3.218E-01	1.137E+00	1.006E+00	6.863E-01
K_{GPP}^{rev}	min^{-1}	1.579E+00	6.797E-01	1.539E-01	1.872E-01	2.996E-01
GPP^{tot}	nM	1.051E+00	5.055E-01	1.581E+00	2.193E+00	2.455E+00
K_{GSK3}^{in}	min^{-1}	1.595E-03	1.595E-03	4.046E-03	1.465E-03	2.495E+00

Table S7. Parameter estimates of the ERK signaling pathway.

Symbol	Unit	ISO	PDGF	AngII	PE	ET-1
K_{inh}^{ERK}	nM	6.174E-03	9.393E-02	1.495E-02	3.353E+00	1.478E-02
K_{inh}^{RKIP}	nM	2.340E-01	9.685E+00	1.732E-01	3.961E-02	1.415E+00
K_{Ras}^{cat}	min^{-1}	2.831E-01	6.828E-01	5.001E+00	1.063E+00	4.664E-02
K_{Raf}^{cat}	nM^{-1} min^{-1}	9.101E-01	1.757E-01	1.942E+00	7.327E-01	3.293E-01
K_{MEK}^{cat}	nM^{-1} min^{-1}	5.070E-01	3.080E+00	9.007E-01	1.588E+00	7.954E-01
K_{ERK}^{cat}	nM^{-1} min^{-1}	1.731E+00	1.214E+01	1.138E+01	1.857E+01	1.364E+01
K_{RKIP}^{cat}	nM^{-1} min^{-1}	4.011E-01	9.475E-02	2.671E-01	6.006E+00	2.069E-01
K_{Ras}^{rev}	min^{-1}	8.632E-01	1.254E+01	6.333E+00	1.249E+00	8.135E-01
K_{Raf}^{rev}	min^{-1}	1.681E+00	3.242E-01	5.400E+00	8.963E+00	2.687E+00
K_{MEK}^{rev}	min^{-1}	1.603E-01	1.978E-01	5.516E-01	6.962E-01	8.752E-01
K_{ERK}^{rev}	min^{-1}	2.479E-02	1.476E-01	6.407E-02	2.820E-01	8.158E-02
K_{RKIP}^{rev}	min^{-1}	1.896E+00	4.323E+00	5.732E-04	5.384E-02	1.733E+00
Ras^{tot}	nM	3.500E-01	3.500E-01	3.500E-01	3.500E-01	3.500E-01
Raf^{tot}	nM	1.200E-01	1.200E-01	1.200E-01	1.200E-01	1.200E-01
MEK^{tot}	nM	3.600E-01	3.600E-01	3.600E-01	3.600E-01	3.600E-01
ERK^{tot}	nM	7.000E-01	7.000E-01	7.000E-01	7.000E-01	7.000E-01
$RKIP^{tot}$	nM	2.400E-01	2.400E-01	2.400E-01	2.400E-01	2.400E-01